Electronic Supplementary Material (ESI) for Journal of Materials Chemistry A.
This journal is © The Royal Society of Chemistry 2021

Rationally Designed Yolk-Shell Co_9S_8-$Co_{1-x}S$ Hollow Spheres for High-Performance Sodium Storage

Yuanyi Luo, Ludi Shi, Huanze He, Guangtao Cong*, Caizhen Zhu*, Jian Xu

Institute of Low-dimensional Materials Genome Initiative, College of Chemistry and Environmental Engineering, Shenzhen University, Shenzhen, Guangdong, 518060, P. R. China.

E-mail: gtcong@szu.edu.cn, czzhu@szu.edu.cn

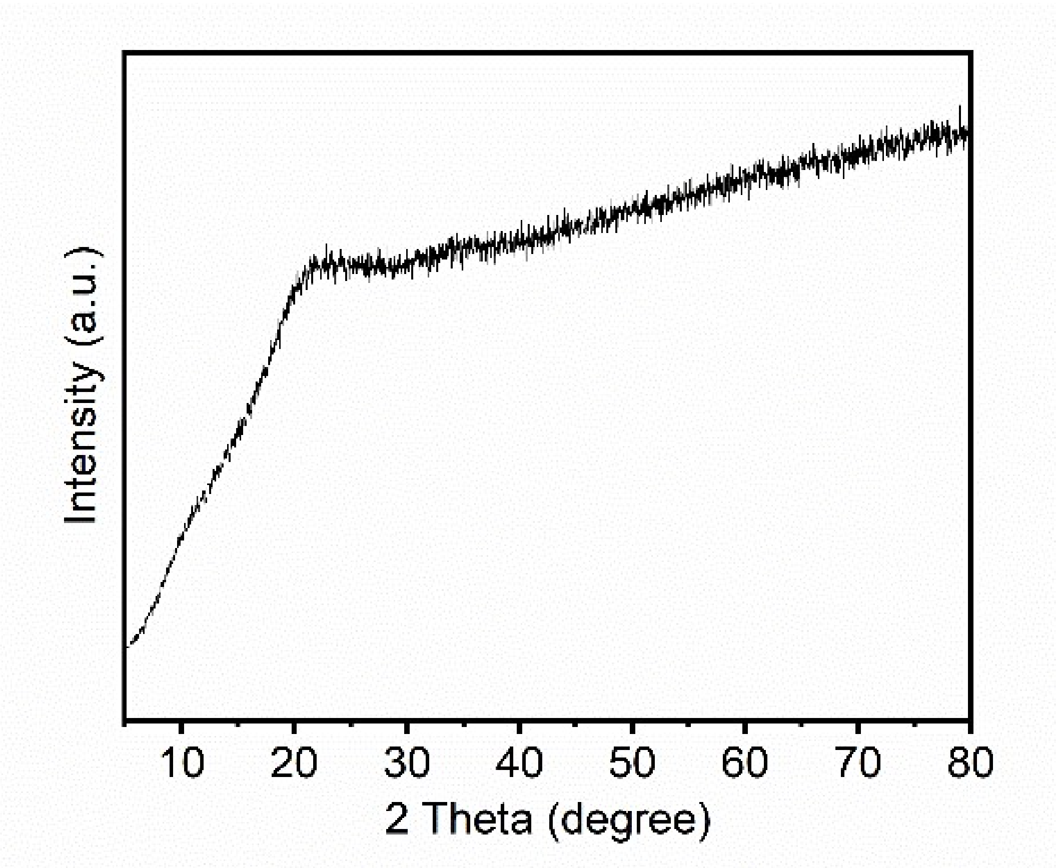

Fig. S1. XRD pattern of Co-G.

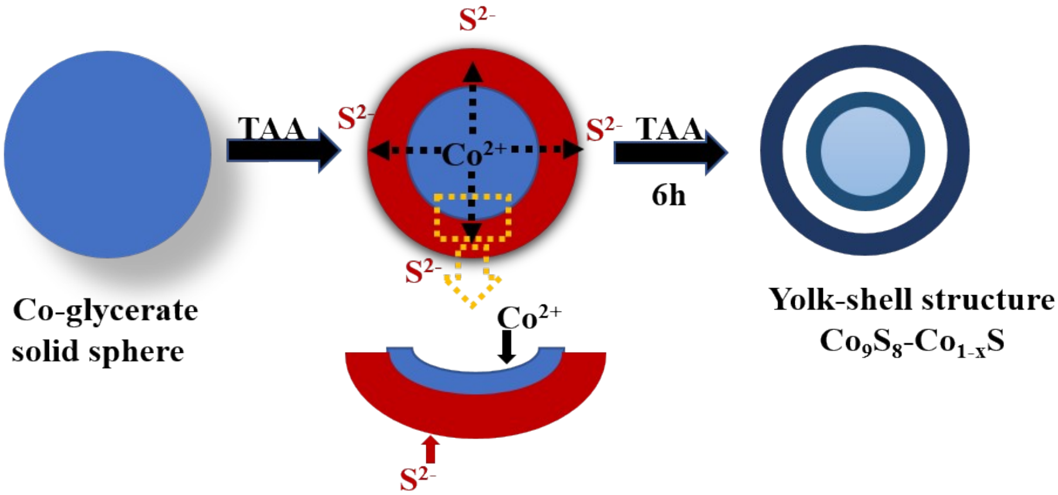

Fig. S2. Schematic illustration of the formation process of yolk-shelled Co_9S_8-$Co_{1-x}S$ hollow spheres.

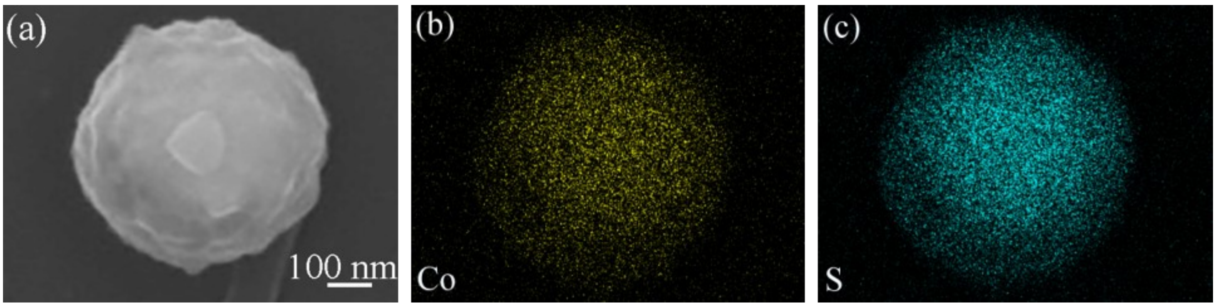

Fig. S3. EDS mapping of Co_9S_8-$Co_{1-x}S$.

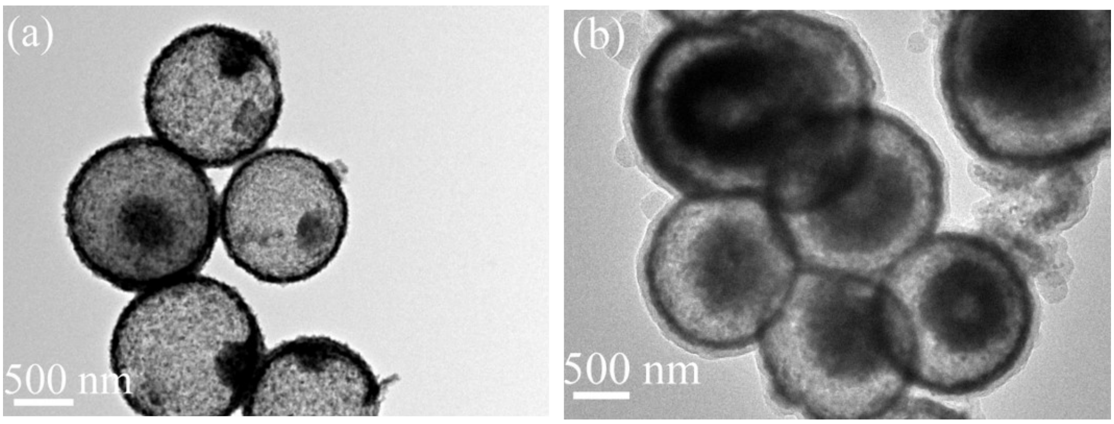

Fig. S4. FESEM of the Co_9S_8-$Co_{1-x}S$ before (a) and after carbonization (b) at 600°C for 2h.

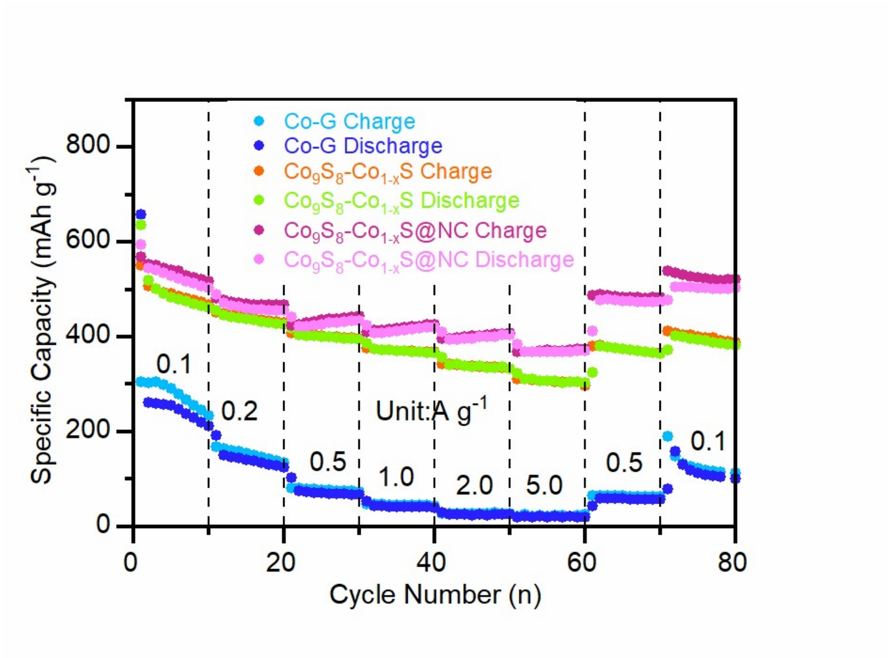

Fig. S5. Rate performance of Co-G, Co_9S_8-$Co_{1-x}S$, and Co_9S_8-$Co_{1-x}S$@NC.

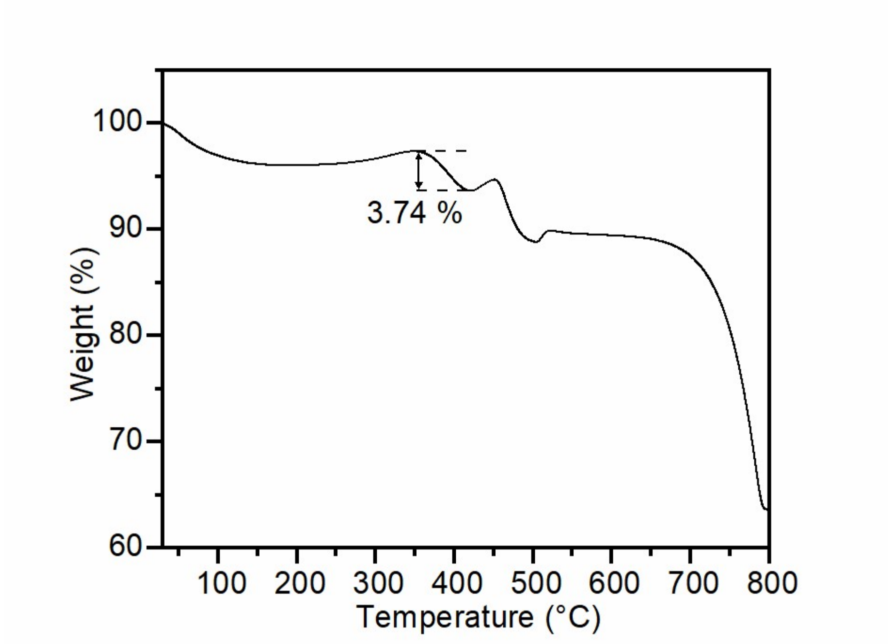

Fig. S6. TGA curves of the Co_9S_8-$Co_{1-x}S$@NC composite.

During the TGA test, the Co_9S_8-$Co_{1-x}S$@NC composite undergoes a multi-step reaction. Co_9S_8-$Co_{1-x}S$ was oxidized to $CoSO_4$, CoO, Co_3S_4 between 200 and 350°C, corresponding to the weight increase in the TGA curve. The weight loss around 400 °C could be ascribed to the gasification of carbon content and the weight fluctuation beyond 450°C could be assigned to the sequential oxidation of CoO to Co_3O_4, Co_3S_4 to Co_3O_4 and $CoSO_4$ to Co_3O_4.[1]

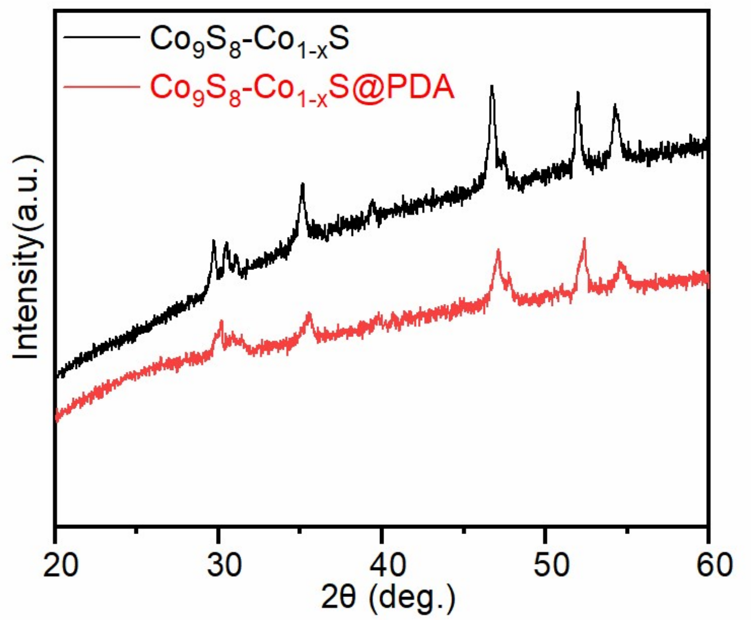

Fig. S7. XRD patterns of the Co_9S_8-$Co_{1-x}S$@NC and Co_9S_8-$Co_{1-x}S$@PDA composites.

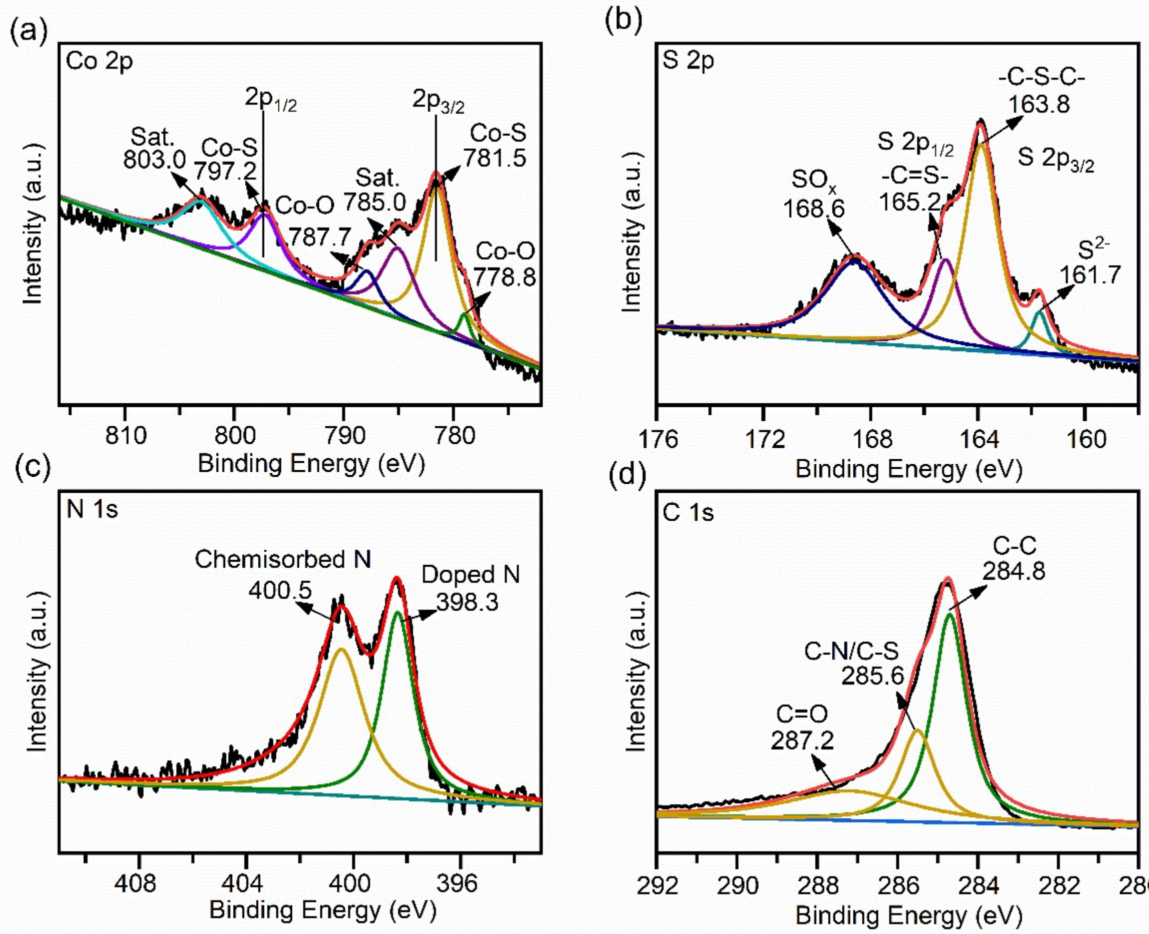

Fig. S8. XPS spectra of Co_9S_8-$Co_{1-x}S$@NC: (a) Co 2p; (b) S 2p; (c) N 1s and (d) C 1s.

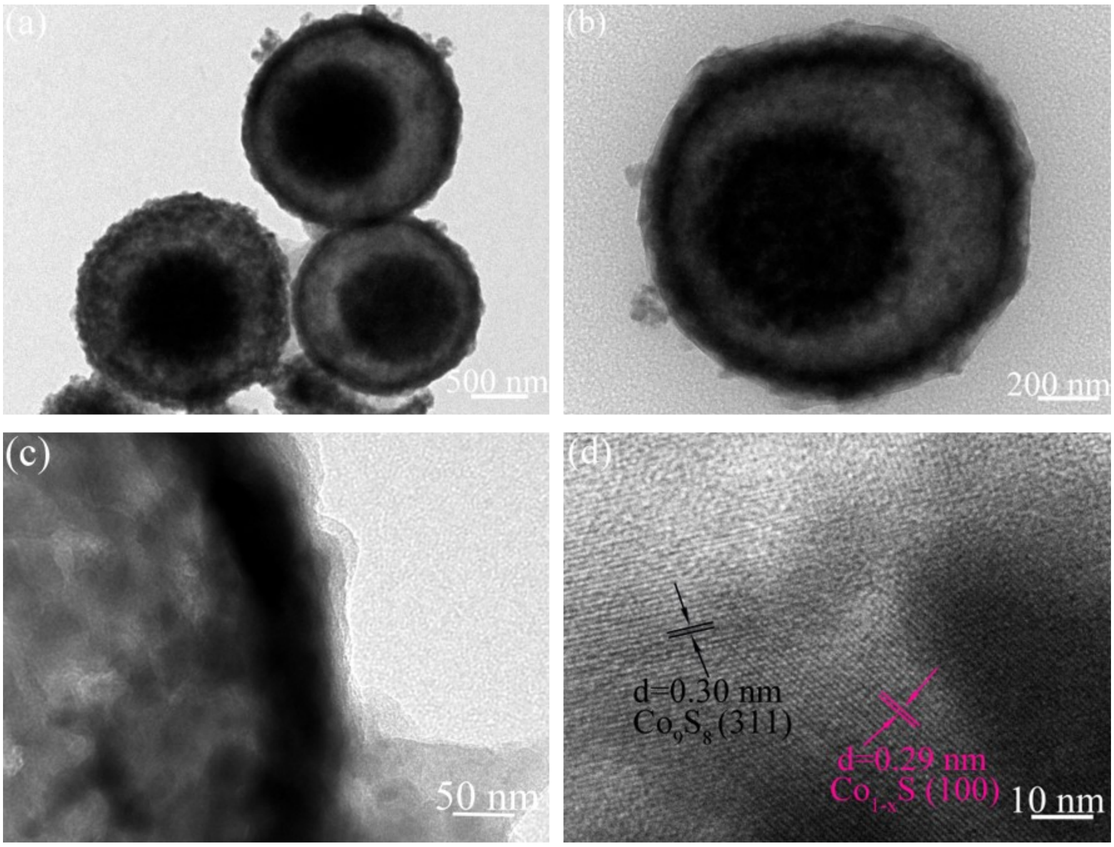

Fig. S9. (a) TEM images of Co_9S_8-$Co_{1-x}S$@NC. (b, c) TEM of an individual Co_9S_8-$Co_{1-x}S$@NC and (d) HRTEM images of (b, c) of Co_9S_8-$Co_{1-x}S$@NC.

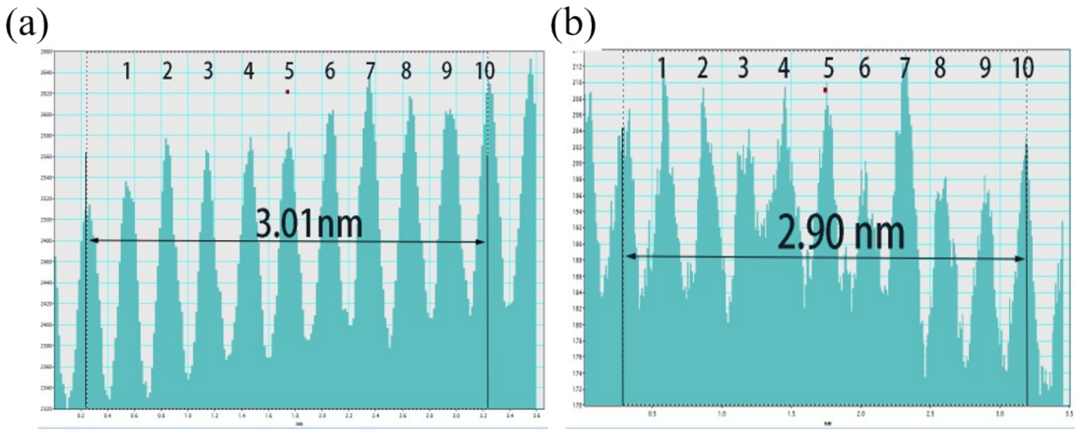

Fig. S10. Intensity profiles of the *d*-spacing in **Fig. S9**d.

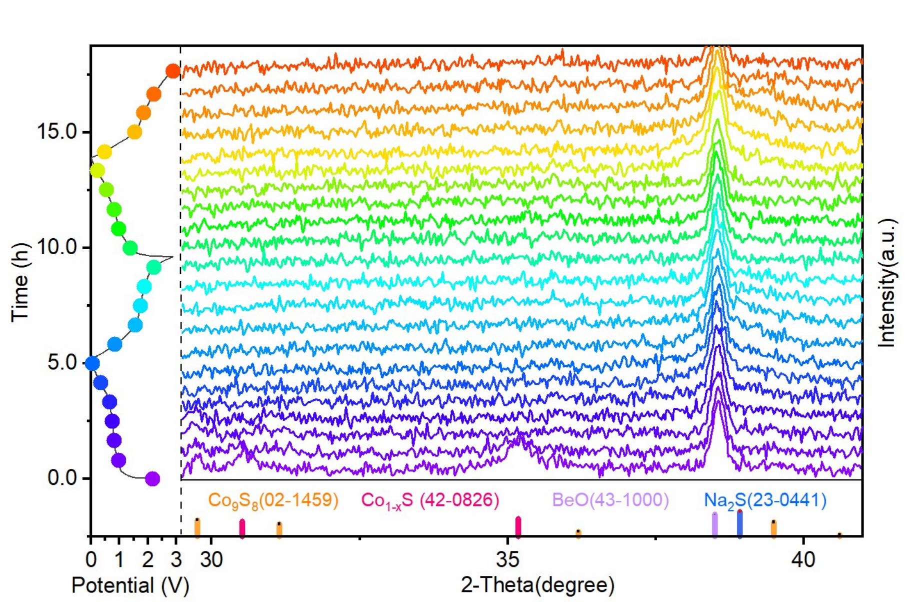

Fig. S11. The peak evolution during the in-situ XRD test.

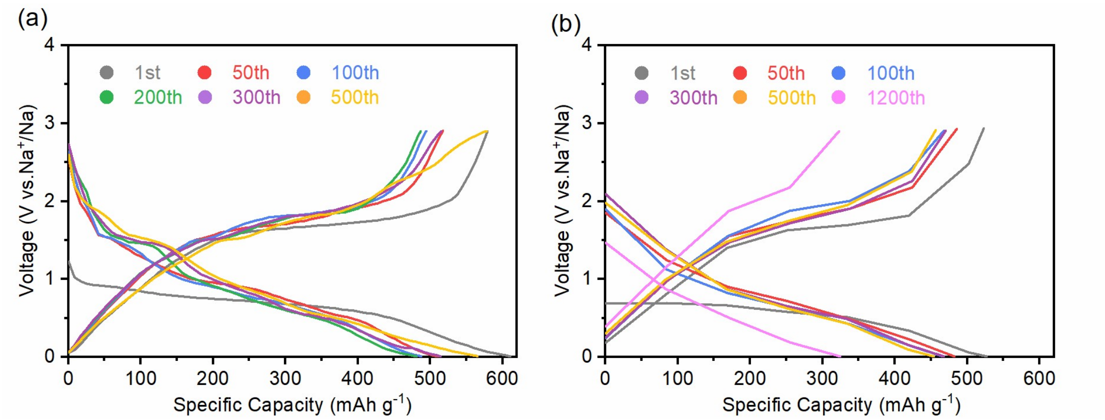

Fig. S12. Galvanostatic voltage profiles at (a) 0.5 A g^{-1} and (b) 5 A g^{-1}.

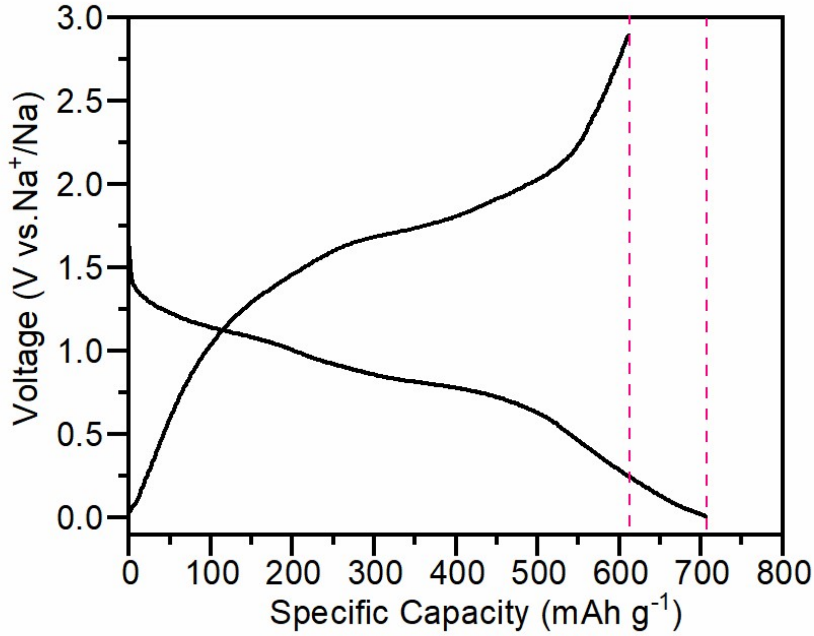

Fig. S13. Initial galvanostatic charge-discharge curves of the bare Co_9S_8-$Co_{1-x}S$ electrode.

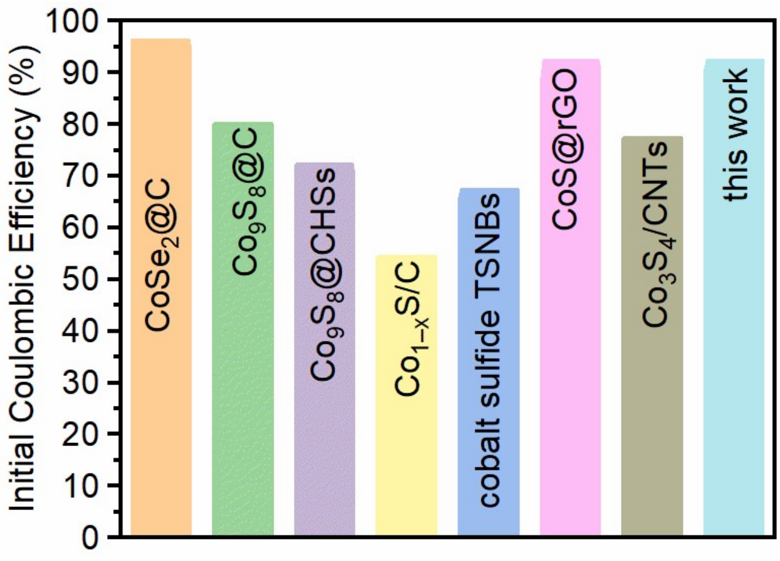

Fig. S14. The ICEs of the Co_9S_8-$Co_{1-x}S$@NC and other reported cobalt-based TMDCs ($CoSe_2$@C: ref.[2], Co_9S_8@C: ref.[3], Co_9S_8@CHSs: ref.[4], $Co_{1-x}S$/C: ref.[5], cobalt sulfide TSNBs: ref.[6], CoS@rGO: ref.[7], Co_3S_4/CNTs: ref.[8])

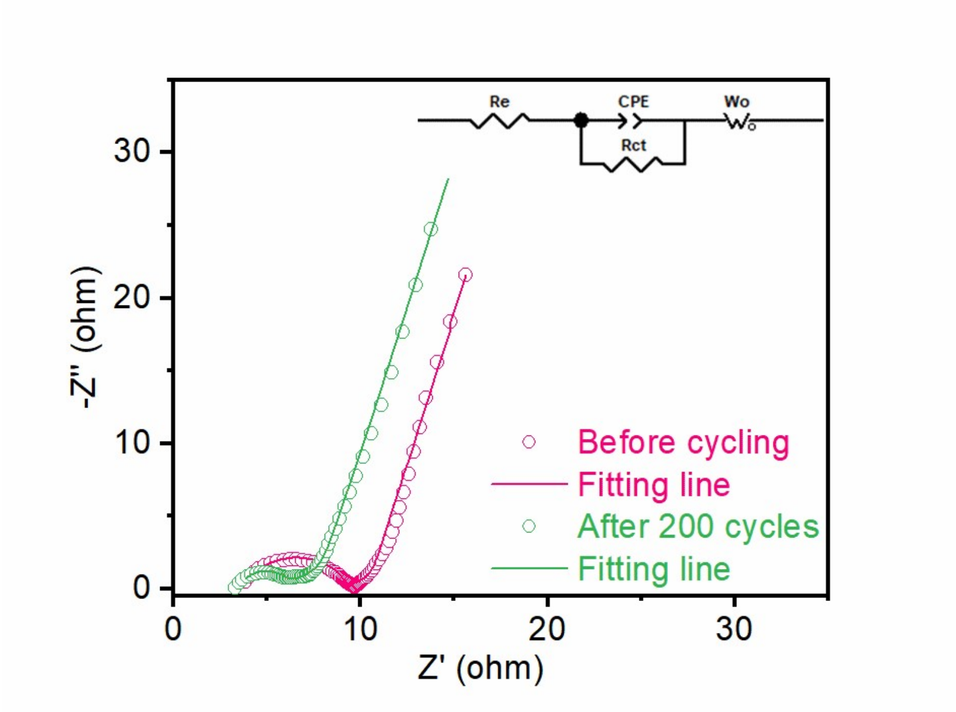

Fig. S15. Experimental and fitted Nyquist curves of Co_9S_8-$Co_{1-x}S$@NC electrode in before cycling and after 200 cycles at 0.5 A g^{-1}. Inset shows the model used to fit the Nyquist curves.

Table S1. Fitted electrochemical impedance parameters of Co_9S_8-$Co_{1-x}S$@NC

Sample		Re	R_{ct}	CPE	
				CPE-T	CPE-P
Co_9S_8-$Co_{1-x}S$@NC	Before cycling	3.812	5.392	9.4794E-6	0.85726
	After 200 cycles	3.510	2.264	4.4677E-6	0.97043

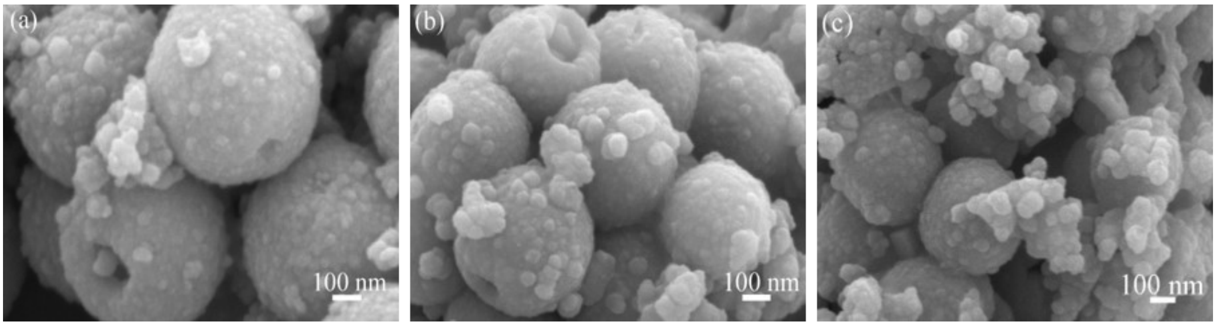

Fig. S16. Ex-situ SEM images of Co_9S_8-$Co_{1-x}S$@NC electrode in (a) before cycling;(b) after 200 cycles;(c) after 500 cycles at 0.5 A g^{-1}.

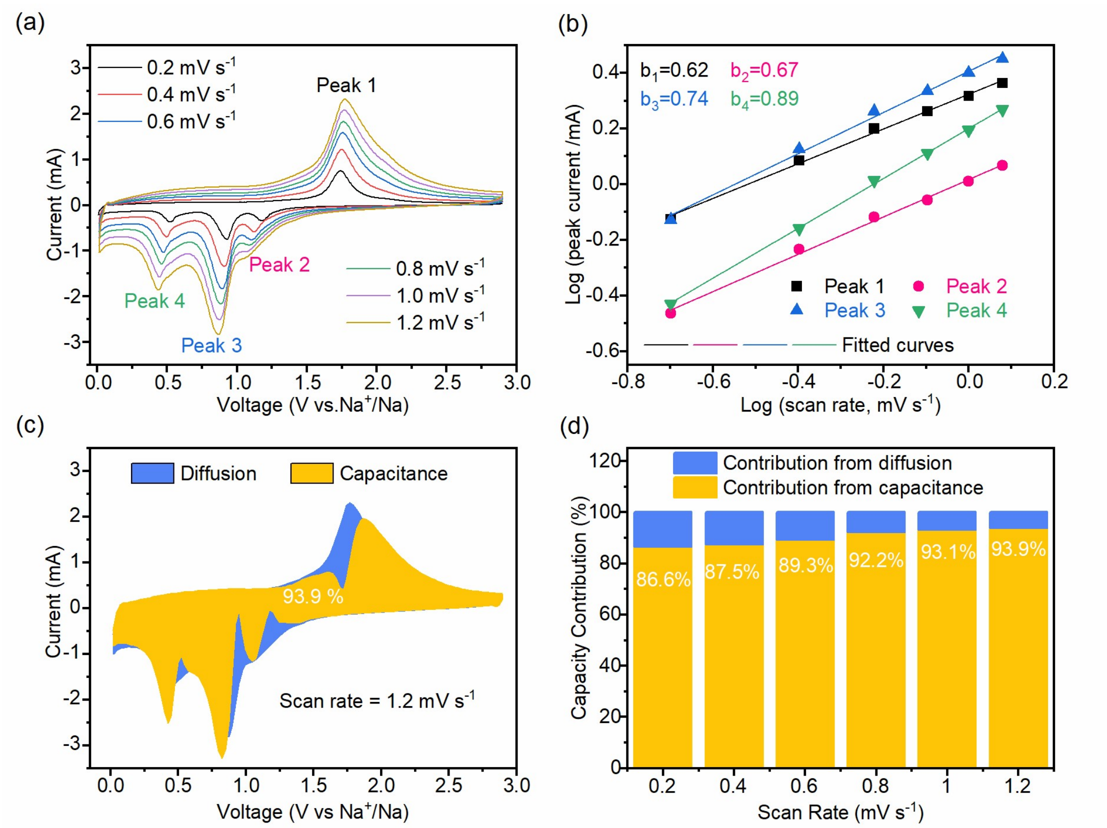

Fig. S17. (a) CV curves of the Co_9S_8-$Co_{1-x}S$@NC electrode at varied scanning rates of from 0.2 to 1.2 mV s^{-1}. (b) The fitted logarithmic relations between scanning rates and peak currents. (c) The pseudo-capacitive contribution (orange area) at 1.2 mV s^{-1}. (d) The pseudo-capacitive contribution at different scanning rates.

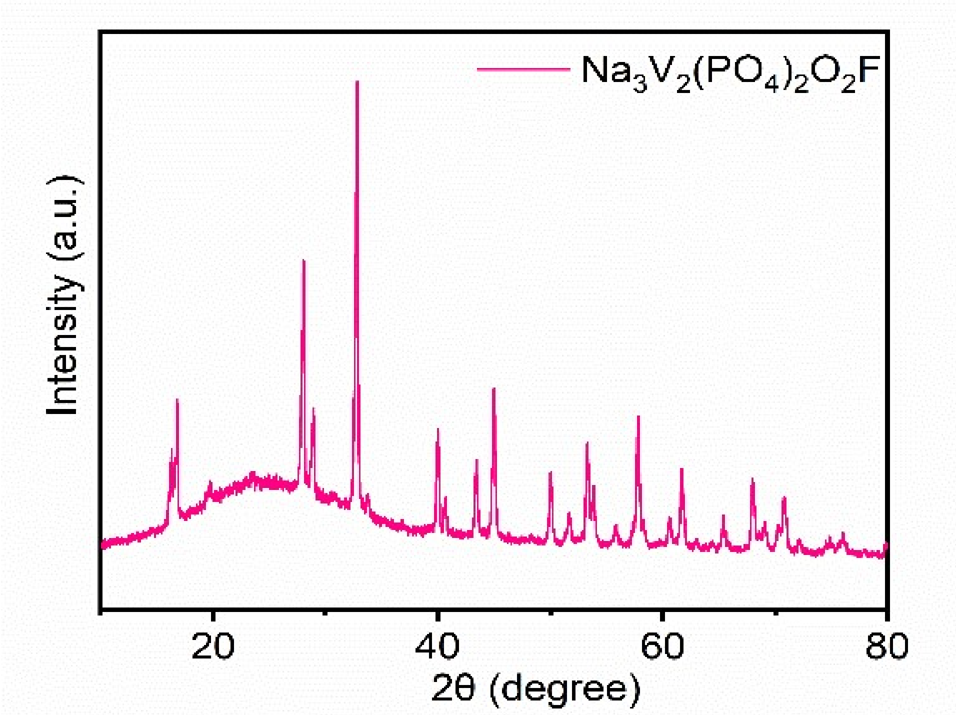

Fig. S18. XRD pattern of the $Na_3V_2(PO_4)_2O_2F$.

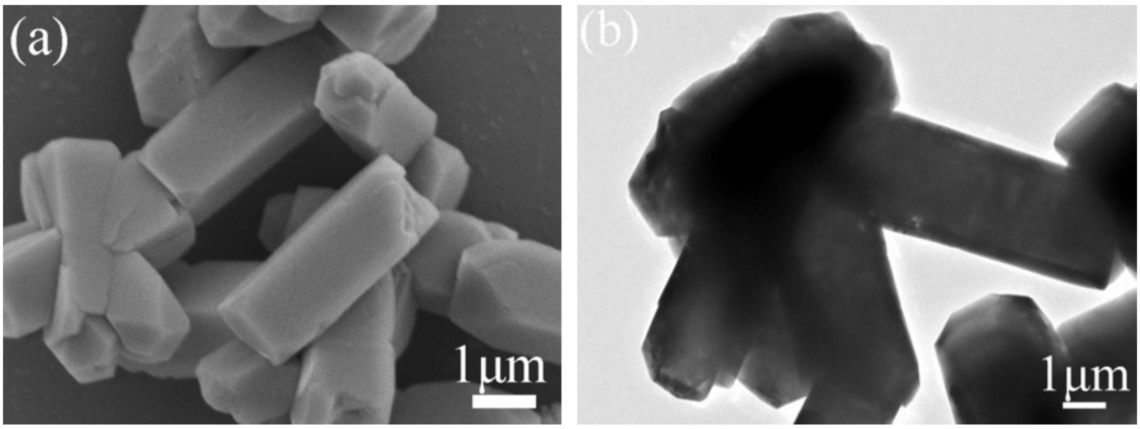

Fig. S19. (a) SEM and (b) TEM images of the $Na_3V_2(PO_4)_2O_2F$.

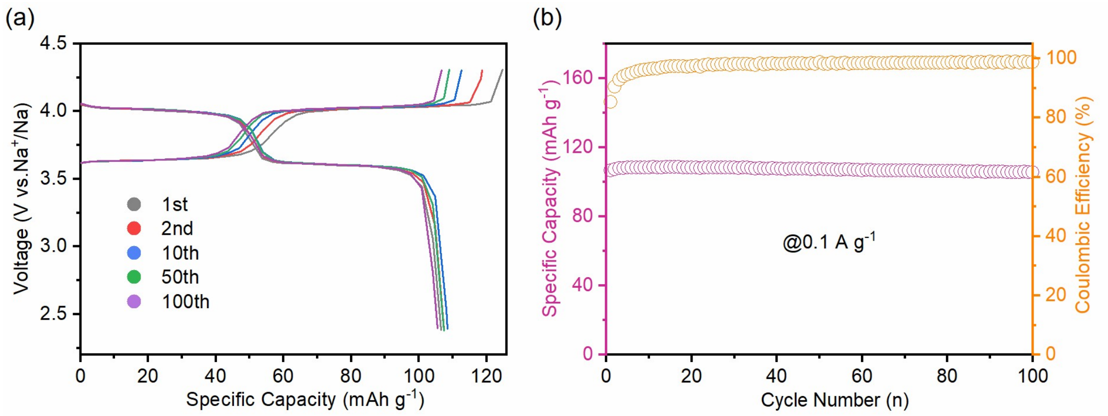

Fig. S20. (a) The galvanostatic discharge-charge curves and (b) cycling performance of the $Na_3V_2(PO_4)_2O_2F$ electrode at 0.1 A g^{-1}.

Table S2 Performance comparison of representative SIB full cells

Anode/cathode	Energy density (Wh/kg)	Reference
Co_9S_8-$Co_{1-x}S$@NC/$Na_3V_2(PO_4)_2O_2F$	~211	This work
NiS@rGO/NVP@C	~154	9
SnS_2/Co_3S_4@CC/$Na_3V_2(PO_4)_2O_2F$	~216	10
1T/2H MoS_2@SnO_2/NVP	~117	11
Sb/$Na_3V_2(PO_4)_3$	~160	12
Sb/$Na_3V_2(PO_4)_2O_2F$	~230	13
$Na_{0.44}MnO_2$-hard carbon	~275	14

Reference

1. Y. Zhang, N. Wang, P. Xue, Y. Liu, B. Tang, Z. Bai and S. Dou, *Chem. Eng.J.*, 2018, **343**, 512-519.
2. Y. Pan, X. Cheng, Y. Huang, L. Gong and H. Zhang, *ACS Applied Materials & Interfaces*, 2017, **9**, 35820-35828.
3. Y. Zhang, N. Wang, P. Xue, Y. Liu, B. Tang, Z. Bai and S. Dou, *Chemical Engineering Journal*, 2018, **343**, 512-519.
4. M. Yin, X. Feng, D. Zhao, Y. Zhao, H. Li, W. Zhou, H. Liu, X. Bai, H. Wang, C. Feng and Q. Jiao, *ACS Sustainable Chemistry & Engineering*, 2019, **7**, 6122-6130.
5. Y. Liu, W. Jiang, M. Liu, L. Zhang, C. Qiang and Z. Fang, *Langmuir*, 2019, **35**, 16487-16495.
6. X. Wang, Y. Chen, Y. Fang, J. Zhang, S. Gao and X. W. Lou, *Angewandte Chemie International Edition*, 2019, **58**, 2675-2679.
7. S. Peng, X. Han, L. Li, Z. Zhu, F. Cheng, M. Srinivansan, S. Adams and S. Ramakrishna, *Small*, 2016, **12**, 1359-1368.
8. D. Liu, A. Hu, Y. Zhu, S. Zhou, Y. Duan, Q. Tang, W. Deng and X. Chen, *Ceramics International*, 2019, **45**, 3591-3599.
9. Y. Luo, L. Shi, H. He, G. Yang, G. Cong, C. Zhu and J. Xu, *Carbon*, 2021, DOI: https://doi.org/10.1016/j.carbon.2021.05.053.
10. L. Cheng, Y. Zhang, P. Chu, S. Wang, Y. Li, X. Ren, P. Zhang and L. Sun, *Journal of Materials Chemistry A*, 2021, **9**, 1630-1642.
11. D. Gui, Z. Wei, J. Chen, L. Yan, J. Li, P. Zhang and C. Zhao, *Journal of Materials Chemistry A*, 2021, **9**, 463-471.
12. F. Wan, J.-Z. Guo, X.-H. Zhang, J.-P. Zhang, H.-Z. Sun, Q. Yan, D.-X. Han, L. Niu and X.-L. Wu, *ACS Appl. Mater. Interfaces*, 2016, **8**, 7790-7799.
13. J.-Z. Guo, P.-F. Wang, X.-L. Wu, X.-H. Zhang, Q. Yan, H. Chen, J.-P. Zhang and Y.-G. Guo, *Adv. Mater.*, 2017, **29**, 1701968.
14. X. Li, P. Yan, M. H. Engelhard, A. J. Crawford, V. V. Viswanathan, C. Wang, J. Liu and V. L. Sprenkle, *Nano Energy*, 2016, **27**, 664-672.